

ηN Final State Interaction in incoherent Photoproduction of η -mesons from the Deuteron near Threshold.

A. Sibirtsev¹, S. Schneider¹, Ch. Elster^{1,2}, J. Haidenbauer¹, S. Krewald¹ and J. Speth¹

¹*Institut für Kernphysik, Forschungszentrum Jülich, D-52425 Jülich*

²*Institute of Nuclear and Particle Physics, Ohio University, Athens, OH 45701*

(July 18, 2018)

Abstract

An analysis of incoherent photoproduction of η mesons off the deuteron for photon energies from threshold to 800 MeV is presented. The dominant contribution, the γN - ηN amplitude, is described within an isobar model. Effects of the final state interactions in the NN as well as the ηN systems are included employing models derived within the meson-exchange approach. It is found that their consideration is important. Specifically, due to an interference effect the influence of the ηN final state interaction is enhanced in the reaction $\gamma d \rightarrow np\eta$ close to threshold.

arXiv:nucl-th/0111086v1 30 Nov 2001

I. INTRODUCTION

Already for a long time the determination of the low energy properties of the ηN interaction has been a challenging subject in meson-nucleon physics. In fact, the actual size of the ηN scattering length is still an open question and there is substantial disagreement between different theoretical predictions.

The knowledge about the low energy behavior of the ηN interaction is extracted either from the analysis of resonance models of the reactions $\pi N \rightarrow \eta N$ and $\gamma N \rightarrow \eta N$ [1–4] or from coupled channel K -matrix [5–8] or T -matrix [9–12] approaches, which in addition include the available information on πN scattering. The current predictions of the imaginary part of the ηN scattering length vary between 0.16 and 0.37 fm, while the variation of the real part ranges from 0.25 to 1.05 fm. Calculations based on an effective Lagrangians approach [13–16] tend to provide scattering lengths on the lower end of the range given above whereas a result from a chiral heavy baryon expansion [17] lies roughly in the middle of this range.

In principle, the ηN interaction could be deduced [18] from η -meson production in nuclear reactions like γ -nucleus, π -nucleus, p -nucleus, or heavy ion collisions. However, in those cases the extracted ηN parameters should be considered as being relevant only for in-medium η -meson scattering and might not represent the vacuum parameters [19]. Thus, the study of η -meson production in few-body systems is certainly more promising with regard to that, specifically because for such reactions a wealth of rather accurate data has become available over the last few years. E.g., the ηN scattering length might be inferred from experiments on $pd \rightarrow {}^3\text{He}\eta$ [20–22] or $np \rightarrow d\eta$ [23,24] by applying models which relate the measured ${}^3\text{He}\eta$ and $d\eta$ scattering length with the one for ηN . In this context it should be noted that both, the $pd \rightarrow {}^3\text{He}\eta$ and $pn \rightarrow d\eta$ measurements, indicate a sizable final state interaction (FSI) due to the η -meson, and thus may be sensitive to the model employed.

Of course it should be expected that also the reactions $pp \rightarrow pp\eta$ [25–28] and $\gamma d \rightarrow np\eta$ data [29] show sensitivity to the ηN FSI for energies near the production threshold. However, it is still an open question whether the analysis of these reactions will allow to pin down the ηN scattering length in a model independent way. Therefore it is important to investigate a larger class of η -production reactions and see to what extent predicted values for the ηN scattering length are compatible with each other.

Here we investigate the effect of the ηN FSI in incoherent photoproduction of η -mesons from the deuteron near threshold. We extend a previous study [30], where the $\gamma d \rightarrow np\eta$ total and differential cross sections were calculated by considering the impulse approximation as well as the neutron-proton (np) FSI. In that work it had turned out that the np FSI can account for a large part of the experimentally observed enhancement of the production cross section near the threshold. However, some discrepancies to the data still remain, specifically at very small excess energies. This discrepancy could be a signal of the ηN FSI and therefore we want to address this question in the present paper. In our previous study we also established that the effect of the np FSI does not depend on the specific model for the nuclear force, since the contributions of intermediate states with large momenta are suppressed through the integration over the deuteron wave function. This feature, specific to the photoproduction reaction on the deuteron, is definitely of advantage if one wants to study the sensitivity of the cross section near threshold to the ηN interaction.

For the ηN FSI we utilize a microscopic model developed by the Jülich group [31,32],

which is a coupled channels model for πN scattering that includes the ηN channel and quantitatively describes the πN phase shifts and inelasticity parameters in both isospin channels for partial waves up to $J = \frac{3}{2}$ and pion-nucleon center-of-mass (c.m.) energies up to 1.9 GeV [32]. Specifically, it provides a realistic description of the quantities relevant for the present investigation, namely the S_{11} πN phase shift and the $\pi N \rightarrow \eta N$ transition cross section. In Section II we give a short introduction to this model, discuss its predictions for the ηN interaction and estimate relevant uncertainties of the model. In Section III we describe the details of our treatment of the np and ηN FSI in the reaction $\gamma d \rightarrow np\eta$. Furthermore, we present our results and analyze the influence of the ηN FSI in detail. Finally, in Section IV, we provide a short summary.

II. ηN INTERACTION

The basic information about the low energy behavior of any interaction is given by the scattering length. Since the enhancement of the η photoproduction cross section is only seen for very low η momenta, one may assume that this enhancement is caused primarily by the low energy behavior of the ηN interaction, and thus by the physics contained in the ηN scattering length $a_{\eta N}$. However, as already discussed in the Introduction, this quantity is not too well determined. A list of currently available values for $a_{\eta N}$ is given in Table I together with the method and reactions involved in the extraction of those values. This compilation¹ clearly indicates that the present status of knowledge about the ηN scattering length is far from being satisfactory.

In our investigation of the influence of the ηN FSI in the η photoproduction reaction we employ a meson-exchange model developed for πN scattering [31,32], which includes the πN - and ηN -channels, and in addition reaction channels which can decay into two pions and a nucleon, namely σN , ρN and $\pi\Delta$. Here σ and ρ are notations for the correlated exchange of two pions in the scalar-isoscalar and vector-isovector channels, respectively. The model describes the πN phase shifts and inelasticities up to 1.9 GeV quantitatively, and also reproduces available data for $\pi^- p \rightarrow \eta n$ differential cross sections. Thus, it is very well suited for the investigation we want to carry out. In particular the model has the advantage that it allows us to calculate the ηN reaction amplitude for any on- as well as off-shell momenta, as it is required for evaluation of the ηN FSI effects, without making additional assumptions.

In Fig. 1 the Feynman diagrams that define the quasi-potential for the πN - ηN and the ηN - ηN transitions are shown. These diagrams are the relevant ones for the calculation of the ηN t-matrix, which is derived within time-ordered perturbation theory in order to have a well-defined off-shell behavior. Further details of the model can be found in Ref. [32]. The πN -channel is coupled with the ηN -channel by the s -channel exchanges of the $N^*(1520)$, $N^*(1535)$, and $N^*(1650)$ baryonic resonances. The exchange of a nucleon in the u -channel

¹We note that in status review [36] of ηN scattering length the results of Ref. [3] were misinterpreted as being extracted from $pd \rightarrow {}^3He n\eta$ data. The ηN scattering length [3,36] actually comes from analysis of the $\pi^- p \rightarrow n\eta$ data.

is also taken into account. In addition, we allow for the exchange of an effective a_0 -meson in the t -channel, representing correlated $\pi\eta$ exchange [33].

Within this model [32], the optimal fit to the πN phase shifts and inelasticities overestimates the total $\pi^- p \rightarrow \eta n$ cross section by roughly 15%. In order to reproduce the $\pi^- p \rightarrow \eta n$ cross section, we have weakened the coupling of the effective a_0 -meson at the $\pi\eta a_0$ vertex. This leads to an underestimation of the πN inelasticities in the S_{11} partial wave in the vicinity of the $N^*(1535)$ resonance. In Ref. [34], this problem is handled by the introduction of an effective $\pi\pi N$ reaction channel, which has quantum numbers that cannot be interpreted by resonant two-pion states, however. One may take the results of Ref. [34] as a hint that the approximate treatment of the three-body dynamics of the $\pi\pi N$ channel by resonances is not adequate. In the context of this work here, we do not try to resolve this problem, but will consider the above mentioned change in the coupling of the a_0 -meson as theoretical uncertainty of our model and discuss its consequences on the size of the low energy ηN parameters and the η photoproduction cross section.

The real and imaginary parts of the scattering amplitude in the ηN partial wave amplitude S_{11} are shown in Fig. 2 as function of the η -meson momentum q given in the ηN c.m. system. The symbols represent the scattering amplitude obtained from the full calculation, while the solid line indicates the effective range expansion of the scattering amplitude with the scattering length $a_{\eta N}$ and effective range $r_{\eta N}$ given by

$$\begin{aligned} a_{\eta N} &= 0.42 + i0.34 \text{ fm} \\ r_{\eta N} &= -2.0 + i0.8 \text{ fm}. \end{aligned} \tag{1}$$

Here the low energy parameters are related to the on-shell ηN scattering amplitude $f(q)$ by

$$f(q) = \left[\frac{1}{a_{\eta N}} + \frac{r_{\eta N} q^2}{2} - iq \right]^{-1}, \tag{2}$$

and $a_{\eta N} = \lim_{q \rightarrow 0} f(q)$. The relation between the ηN scattering amplitude and $t_{\eta N}$ -matrix is given in our normalization as

$$f(q) = -\pi \frac{\sqrt{q^2 + m_N^2} \sqrt{q^2 + m_\eta^2}}{\sqrt{q^2 + m_N^2} + \sqrt{q^2 + m_\eta^2}} t_{\eta N}(q, q), \tag{3}$$

where m_N and m_η are the nucleon and η -meson masses, respectively. In order to show the dependence of the ηN scattering amplitude on the low energy parameters, the dashed line in Fig. 2 gives the effective range expansion of f with the parameters of Ref. [8], namely

$$\begin{aligned} a_{\eta N} &= 0.75 + i0.27 \text{ fm} \\ r_{\eta N} &= -1.5 - i0.24 \text{ fm}. \end{aligned} \tag{4}$$

It is very clear that the two different scattering amplitudes exhibit a substantial difference both in absolute value and in the momentum dependence of the ηN scattering amplitude.

Table I indicates that the ηN interaction is frequently described in a resonance model approach. In order to demonstrate the strong interplay between resonant and non-resonant

contributions in the case of the Jülich model we isolate the resonant piece and compare its amplitude to the one given by the full model. The solid symbols in Fig. 3 indicate the real (dots) and imaginary (squares) part of the $\eta N S_{11}$ partial wave scattering amplitude calculated with the $N^*(1535)$ resonance alone. The solid lines represent the total ηN scattering amplitude given by the effective range expansion with the parameters of Eq. (1) and correspond to the solid lines in Fig. 2. This comparison clearly shows that the non-resonant contribution is quite large at small momenta $q \leq 300$ MeV/c, and thus the interplay between resonant and non-resonant contributions is very important for the scattering length.

III. THE REACTION $\gamma D \rightarrow NP\eta$.

The lowest order contributions for the reaction $\gamma d \rightarrow np\eta$ are depicted in Fig. 4. In our previous study [30] of this reaction we considered the production of η mesons via the dominant $S_{11}(1535)$ resonance (impulse approximation), shown in Fig. 4a, and the np FSI as indicated in Fig. 4b. The explicit details of the model for the direct production are given in Ref. [30], and will only be briefly summarized here. Using the impulse approximation (IA) the amplitude \mathcal{M}_{IA} of the reaction $\gamma d \rightarrow np\eta$ for given spin S and isospin T of the final nucleons can be written as

$$\mathcal{M}_{IA} = A^T(s_1)\phi(p_2) - (-1)^{S+T} A^T(s_2)\phi(p_1). \quad (5)$$

Here $\phi(p_i)$ stands for the deuteron wave function, p_i ($i = 1, 2$) is the momentum of the proton or neutron in the deuteron rest frame, and A^T denotes the isoscalar or isovector η -meson photoproduction amplitude at the squared invariant collision energy s_N given by

$$s_N = s - m_N^2 - 2(E_\gamma + m_d)E_N + 2\vec{k}_\gamma \cdot \vec{p}_i. \quad (6)$$

The photon momentum is given by \vec{k}_γ . Details of the photoproduction amplitude A^T are described in Ref. [30].

The result for the total cross section for the reaction $\gamma d \rightarrow np\eta$ based on the impulse approximation is shown as dotted line in Fig. 5 in comparison to experiment [29]. The cross section is shown as a function of the photon beam energy E_γ (lower axis) as well as a function of the excess energy (upper axis). Here the excess energy is defined as

$$\epsilon = \sqrt{s} - m_p - m_n - m_\eta, \quad (7)$$

with the invariant mass $s = m_d^2 + 2m_d E_\gamma$. The particle masses adopted in our calculations are $m_d = 1875.61339$ MeV, $m_p = 938.27231$ MeV, $m_n = 939.56563$ MeV and $m_\eta = 547.3$ MeV. We explicitly indicate the masses with the available accuracy, since the excess energy depends on those values, and thus the accuracy is important for the analysis of the data especially very close to the reaction threshold. The comparison with experiment shows that the impulse approximation reproduces the data well for excess energies $\epsilon \geq 50$ MeV, however there is a clear underprediction of the data for energies closer to threshold.

In the next order of the scattering expansion, the FSI in the nucleon-nucleon (NN) system and the η -nucleon system need to be considered. The effect of the FSI in the NN

channel is expected to be the stronger one, and was already studied previously [30], but for completeness we repeat the essential ingredients here. The amplitude describing the NN FSI can be written as

$$\mathcal{M}_{NN} = t_{NN} g_{NN} A^T. \quad (8)$$

Here t_{NN} denotes the half-shell np scattering matrix and g_{NN} the two nucleon propagator. Explicitly, the amplitude for the diagram shown by Fig. 4b is given by

$$\mathcal{M}_{NN} = m_N \int dk k^2 \frac{t_{NN}(q, k) A^T(s'_N) \phi(p'_N)}{q^2 - k^2 + i\epsilon}, \quad (9)$$

with q being the nucleon momentum in the final np system and

$$\vec{p}'_N = \vec{k} + \frac{\vec{k}_\gamma - \vec{p}_\eta}{2}. \quad (10)$$

Here p_η represents the η -meson momentum and $p'_N = |\vec{p}'_N|$. The half-shell np scattering matrix in the 1S_0 and 3S_1 partial waves $t_{NN}(q, k)$ is obtained at corresponding off-shell momenta k from the CD-Bonn potential [35], which describes the NN data base with a χ^2/datum of about 1. However, as already pointed out in Ref. [30], all modern, high precision NN interaction would give the same result, since due to the integration over the deuteron wave function in Eq. (9) possible off-shell differences in the NN potentials are strongly suppressed.

The amplitude with the η -N FSI is graphically represented in Fig. 4c and given as

$$\mathcal{M}_{\eta N} = t_{\eta N} g_{\eta N} A^T, \quad (11)$$

where $t_{\eta N}$ is the half-shell ηN scattering matrix. The ηN propagator is indicated by $g_{\eta N}$. Explicitly, the amplitude is written as

$$\mathcal{M}_{\eta N} = \frac{m_N m_\eta}{m_N + m_\eta} \int dk k^2 \frac{t_{\eta N}(q, k) A^T(s''_N) \phi(p''_N)}{q^2 - k^2 + i\epsilon}. \quad (12)$$

The η -meson momenta in the final and intermediate state of the ηN system are given by q and k , ϕ stands for the deuteron s-wave, and $t_{\eta N}(q, k)$ is the half-shell ηN scattering matrix in the S_{11} partial wave, and

$$\vec{p}''_N = \vec{k} + \frac{m_N (\vec{k}_\gamma - \vec{p}_N)}{m_N + m_\eta}, \quad (13)$$

where \vec{p}_N is the momentum of the outgoing proton or neutron in the deuteron rest frame.

The total cross section $\gamma d \rightarrow np\eta$ including the np and ηN FSI in s-waves is displayed in Fig. 5. The dashed line shows the result for the impulse approximation plus np FSI. As pointed out in Ref. [30], the consideration of the np FSI alone provides already an almost satisfactory description of the experimental cross section for small excess energies. The additional consideration of the ηN FSI as given by the meson-baryon model described in Section II leads to the solid line in Fig. 5. As expected, the ηN FSI enhances the cross section very close to the reaction threshold. However, for excess energies in the range of

$10 \geq \epsilon \geq 40$ MeV the presently available experimental values are slightly overpredicted. We also observe that for excess energies larger than 40 MeV there is no effect of the ηN FSI anymore. The same is true for the np FSI.

It is illuminating to look at the difference in the relative strength of the two different final state interactions and their possible interference in our full calculation of the η photoproduction cross section. For a more detailed insight, we plot in Fig. 6 the ratio of calculations with the final state interactions included separately to the calculation based on the impulse approximation alone. The dotted line in Fig. 6 represents the calculation including only the ηN FSI, the dashed line only the NN FSI. From this, it is clear that the NN FSI is the dominant one. The ratio of the full calculation containing both, the ηN and NN FSI, to the impulse approximation is given by the solid line. A comparison to the two other curves shows that the two final state interactions interfere constructively at small excess energies, which magnifies the effect of the relatively weak ηN FSI.

In order to study the effects of the ηN interaction close to the reaction threshold in more detail, we divide the experimental points by our calculation containing the IA and the np FSI, i.e. the result of the dashed line in Fig. 5. Now the enhancement in the cross section for the reaction $\gamma d \rightarrow np\eta$ close to the threshold becomes visible by a deviation from one for excess energies $\epsilon \leq 30$ MeV, cf. Fig. 7. This enhancement, which is present in the data, is seen in the full calculation containing the ηN FSI as well. The solid line of Fig. 5 corresponds to the lower bound of the shaded band in Fig. 7. The ηN interaction discussed in Section II leads to a scattering length $a_{\eta N} = 0.42 + i0.34$ fm (cf. Eq. (1)). Since this model leads to a slight overprediction of the $\pi^- p \rightarrow \eta n$ cross section we have produced a variant model that also fits the data (cf. the discussion in Section II). In the latter model the ηN interaction is somewhat more attractive, leading to a scattering length of $a_{\eta N} = 0.54 + i0.18$. The corresponding total cross section for the reaction $\gamma d \rightarrow np\eta$ is given in Fig. 7 by the upper bound of the shaded area. Consequently, the shaded area in Fig. 7 can be seen as a reflection of the theoretical uncertainty in the ηN interaction arising within the Jülich meson-baryon model.

Indeed, it is interesting to explore more thoroughly how strongly our calculation of the ηN FSI depends on the specific properties of the ηN interaction. In order to study whether there is sensitivity to the off-shell behavior we carried out calculations where the ηN amplitude is replaced by its effective range expansion of Eq. (2), i.e. basically by the on-shell ηN t-matrix. (Note that the quality of the effective range expansion as compared to the full ηN t-matrix is shown in Fig. 2.) Surprisingly, we obtained identical results for the η photoproduction cross section when using either the ηN t-matrix from the effective range expansion or the one from the full model. This can be explained through the relatively good representation of the ηN scattering amplitude by the effective range expansion for quite a large momentum range as is illustrated in Figs. 2 as well as a very weak k -dependence of the half-shell ηN t-matrix, $t_{\eta N}(q, k)$. As an aside, we want to emphasize that an argument along the same line with respect to the np FSI and its effective range expansion is not valid, since the energy dependence as well as the dependence on the off-shell momentum of the NN t-matrix is much stronger.

The next logical step is to see whether even more quantitative information about the strength of the ηN interaction at low energies can be extracted. Since we found that the ηN amplitude obtained with the effective range expansion of Eq. (2) is numerically identical to

the full calculation of the amplitude, Eq. (12), we can explore the effect of different values for the ηN low energy parameters on the cross section of the reaction $\gamma d \rightarrow np\eta$ close to threshold. Our studies could establish that the calculations of the η -photoproduction cross section are not sensitive to the effective range parameter $r_{\eta N}$ of Eq. (2), leaving the only sensitivity to the scattering length $a_{\eta N}$. In Fig. 7 we display two calculations with scattering lengths $a_{\eta N}=0.25+i0.16$ fm [2] (dashed line) and $a_{\eta N}=0.74+i0.27$ fm [7] (dash-dotted line). The figure suggests that the presently available data for the total cross section for $\epsilon \leq 40$ MeV show a preference for a smaller value of the ηN scattering length. Obviously more precise data are highly desirable to confirm these indications. Since the calculations with different values for $a_{\eta N}$ involve differences in the real as well as imaginary part of the scattering length, we investigated which of the two is mainly responsible for the effects shown in Fig. 7 and found that the major contribution to the size of the ηN FSI in this reaction stems from the interference of the real part of $a_{\eta N}$ with the NN FSI.

IV. SUMMARY

We calculated the reaction $\gamma d \rightarrow np\eta$ including the dominant contribution by the $S_{11}(1535)$ resonance and the final state interactions between all outgoing particles. Those final state interactions influence the cross section for inclusive photoproduction of η mesons only for excess energies of the η -meson smaller than 40 MeV. At higher energies the cross section is solely given by the impulse approximation.

The FSI between the outgoing nucleons is essential to bring the calculated cross section into the vicinity of the experimental values. Due to an interference effect the ηN final state interaction provides an additional enhancement of the production cross section at energies close to threshold as required by the data. We found that the effect of the FSI resulting from the ηN interaction can be well incorporated into the model calculation by resorting to an effective range expansion fitted to the scattering amplitude of the ηN model. Guided by this finding, we considered ηN final state interactions given by effective range expansions with different values for the scattering length and conclude that the presently available cross section measurement for the reaction $\gamma d \rightarrow np\eta$ favor moderate values of the real part of the scattering length $a_{\eta N}$.

ACKNOWLEDGMENTS

This work was performed in part under the auspices of the U. S. Department of Energy under contract No. DE-FG02-93ER40756 with the Ohio University. The authors appreciate valuable discussions with B. Krusche, V. Metag and H. Ströher on the subject. One of the authors (S.K.) wants to thank the Research Center for the Subatomic Structure of Matter (CSSM) at the University of Adelaide for the warm hospitality during a recent visit, and acknowledges support by grant No. 447AUS113/14/0 by the Deutsche Forschungsgemeinschaft.

REFERENCES

- [1] R.S. Bhalerao and L.C. Liu, Phys. Rev. Lett. **54**, 865 (1985).
- [2] C. Bennhold and H. Tanabe, Nucl. Phys. A **530**, 625 (1991).
- [3] C. Wilkin, Phys. Rev. C **47**, R938 (1993).
- [4] G. Fäldt and C. Wilkin, Nucl. Phys. A **587**, 769 (1995).
- [5] Ch. Saueremann, B.L. Friman and W. Nörenberg, Phys. Lett. B **341**, 261 (1995).
- [6] Ch. Deutsch-Saueremann, B.L. Friman and W. Nörenberg, Phys. Lett. B **409**, 51 (1997).
- [7] A.M. Green and S. Wycech, Phys. Rev. C **55**, R2167 (1997).
- [8] A.M. Green and S. Wycech, Phys. Rev. C **60**, 035208 (1999).
- [9] M. Arima, K. Shimizu and K. Yazaki, Nucl. Phys. A **543**, 613 (1992).
- [10] M. Batinić, I. Slaus, A. Svark, B.M.K. Nefkens, Phys. Rev. C **51**, 2310 (1995); M. Batinić, I. Slaus, A. Svark, Phys. Rev. C **52**, 2188 (1995).
- [11] V.V. Abaev and B.M.K. Nefkens, Phys. Rev. C **53**, 385 (1996).
- [12] M. Batinić, I. Slaus, A. Svark, B.M.K. Nefkens, T.S.H. Lee, Physica Scripta **58**, 15 (1998).
- [13] N. Kaiser, P.B. Siegel and W. Weise, Phys. Lett. B **362**, 23 (1995).
- [14] N. Kaiser, T. Waas and W. Weise, Nucl. Phys. A **612**, 297 (1997).
- [15] J. Caro Ramon, N. Kaiser, S. Wetzell and W. Weise, Nucl. Phys. A **672**, 249 (2000).
- [16] J. Nieves and E. Ruiz Arriola, Phys. Rev. D **64**, 116008 (2001).
- [17] B. Krippa, Phys. Rev. C **64**, 047602 (2001).
- [18] T.H. Bauer, R.D. Spital and D.R. Yennie, Rev. Mod. Phys., **50**, 261 (1978)
- [19] M. Effenberger and A. Sibirtsev, Nucl. Phys. A **632**, 99 (1998).
- [20] B. Mayer et al., Phys. Rev. C **53**, 2068 (1996).
- [21] M. Betigeri et al., Phys. Lett. B **472**, 267 (2000).
- [22] W. Klimala et al., Acta Phys. Polon. B **31**, 2231 (2000).
- [23] H. Calén et al., Phys. Rev. Lett. **79**, 2642 (1997).
- [24] H. Calén et al., Phys. Rev. Lett. **80**, 2069 (1998).
- [25] E. Chiavassa et al., Phys. Lett. B **322**, 270 (1994).
- [26] H. Calén et al., Phys. Lett. B **366**, 39 (1996).
- [27] A.M. Bergdolt et al., Phys. Rev. D **48**, R2969 (1993).
- [28] J. Smyrski et al., Phys. Lett. B **474**, 182 (2000).
- [29] B. Krusche et al., Phys. Lett. B **358**, 40 (1995).
- [30] A. Sibirtsev, Ch. Elster, J. Haidenbauer and J. Speth, Phys. Rev. C **64**, 024006.
- [31] C. Schütz, J. Haidenbauer, J. Speth, and J.W. Durso, Phys. Rev. C **57**, 1464 (1998).
- [32] O. Krehl, C. Hanhart, S. Krewald, J. Speth, Phys. Rev. C **62**, 025207 (2000).
- [33] G. Janssen, B.C. Pearce, K. Holinde, and J. Speth, Phys. Rev. D **52**, 2690 (1995).
- [34] T. Feuster and U. Mosel, Phys. Rev. C **59**, 460(1999).
- [35] R. Machleidt, Phys. Rev. C **63**, 024001 (2001).
- [36] A.M. Green and S. Wycech, Phys. Rev. C **55**, 2167 (1997).

TABLES

TABLE I. Compilation of different values for the ηN scattering length $a_{\eta N}$ as evaluated by resonance models (RM), T- or K-matrix approaches or chiral effective Lagrangians (χ EL). The reference in the table shows only the first author together with the year of publication. The channels included in the analyses are also listed.

$a_{\eta N}$ (fm)	Reference	Year	Model	Channels
$0.27 + i0.22$	Bhalerao [1]	1985	RM	$\pi N \rightarrow \pi N, \eta N, \pi \Delta$
$0.25 + i0.16$	Bennhold [2]	1991	RM	$\pi N \rightarrow \pi N, \eta N,$ $\rightarrow \pi \pi N; \gamma N \rightarrow \eta N$
$0.98 + i0.37$	Arima [9]	1992	T	$\pi N \rightarrow \pi N, \eta N$
$0.55 + i0.30$	Wilkin [3]	1993	FSI	$\pi N \rightarrow \eta N$
$0.51 + i0.21$	Sauermann [5]	1995	K	$\pi N \rightarrow \pi N, \eta N$
$0.68 + i0.24$	Kaiser [13]	1995	χ EL	$\pi N \rightarrow \pi N, \eta N,$ $\rightarrow K \Lambda, K \Sigma$
$0.888 + i0.279$	Batinić [10]	1995	T	$\pi N \rightarrow \pi N, \eta N$
$0.476 + i0.279$	Fäldt [4]	1995	RM	$\pi N \rightarrow \eta N$ $\gamma N \rightarrow \eta N$
$0.621 + i0.306$	Abaev [11]	1996	T	$\pi N \rightarrow \eta N$ $\bar{K} N \rightarrow \eta \Lambda$
$0.51 + i0.21$	Deutsch-Sauermann [6]	1997	K	$\pi N \rightarrow \pi N, \eta N$ $\gamma N \rightarrow \pi N, \eta N$
$0.20 + i0.26$	Kaiser [14]	1997	χ EL	$\pi N \rightarrow \pi N, \eta N,$
$0.74 + i0.27$	Green [7]	1997	K	$\pi N \rightarrow \pi N, \eta N$ $\gamma N \rightarrow \pi N, \eta N$
$0.717 + i0.263$	Batinić [12]	1998	T	$\pi N \rightarrow \pi N, \eta N$
$0.87 + i0.27$	Green [7]	1999	K	$\pi N \rightarrow \pi N, \eta N$ $\gamma N \rightarrow \pi N, \eta N$
$1.05 + i0.27$	Green [8]	1999	K	$\pi N \rightarrow \pi N, \eta N$ $\gamma N \rightarrow \pi N, \eta N$
$0.32 + i0.25$	Caro Ramon [15]	2000	χ EL	$\pi N \rightarrow \pi N, \eta N,$
$0.772 + i0.217$	Nieves [16]	2001	χ EL	$\pi N \rightarrow \pi N, \eta N, K \Lambda, K \Sigma$
$0.54 + i0.49$	Krippa [17]	2001	χ EL	$\pi N \rightarrow \pi N, \eta N$
$0.42 + i0.34$	present work (Krehl [32])	2001	T	$\pi N \rightarrow \pi N, \eta N, \text{etc.}$

FIGURES

FIG. 1. The Feynman diagrams of the meson-baryon model that constitute the Born terms for the transitions in the $\pi N\text{-}\eta N$ and the $\eta N\text{-}\eta N$ channels.

FIG. 2. The real and imaginary parts of the ηN scattering amplitude f in the S_{11} partial wave as function of the c.m. momentum q . The symbols show the results of the Jülich meson-baryon model [32]. The circles stand for the real part, while the squares indicate the imaginary part. The solid lines show the effective range expansion using the parameters of Eq. 1. The dashed lines indicate the effective range expansion with parameters of Eq. 4 from Ref. [8].

FIG. 3. The real and imaginary parts of the ηN scattering amplitude f in the S_{11} partial wave as function of the c.m. momentum q showing the contribution from the $N^*(1535)$ resonance of the Jülich meson-baryon model [32]. The circles stand for the real part of f , while the squares show the imaginary part. As a guide to the eye, the solid lines indicate the effective range expansion given by the full model, as is shown by the Fig. 1.

FIG. 4. The diagrams for the reaction $\gamma d \rightarrow np\eta$: (a) impulse approximation (IA), (b) IA with NN final state interaction represented by the NN t-matrix, and (c) IA and ηN final state interaction. Here A denotes the $\gamma N\text{-}\eta N$ transition operator.

FIG. 5. The total cross section for inclusive photoproduction of η -mesons off deuterium as function of the photon energy E_γ (lower axis) and the excess energy ϵ (upper axis). The experimental data are taken from Ref. [29]. The dotted line shows our IA calculation [30], while the dashed line is the result with np final state interaction. The solid line shows the full result, including the ηN final state interaction from the Jülich meson-baryon model.

FIG. 6. The cross section ratios for inclusive photon production of η -mesons off the deuteron as a function of the excess energy ϵ . Shown are our calculations including the indicated final state interactions divided by our calculation [30] based on the impulse approximation (dotted line in Fig. 6). The solid line indicates the full calculation containing np and ηN FSI. The dashed line stands for a calculation including only the np FSI, whereas the calculation for the dotted line includes only the ηN FSI.

FIG. 7. The cross section ratios for inclusive photon production of η -mesons off the deuteron as a function of the excess energy ϵ . Shown is the experimental cross section divided by our calculation [30] containing IA and np FSI (dashed line of Fig. 6). The solid line indicates the full calculations containing the ηN FSI divided by the calculation containing IA and np FSI. The dash-dotted and dashed lines show the calculations with ηN scattering lengths $a_{\eta N}=0.74+i0.27$ fm and $a_{\eta N}=0.25+i0.16$ fm, respectively. The hatched area indicate the uncertainty of the calculations with the ηN FSI taken from the Jülich meson-baryon model, as discussed in the text.

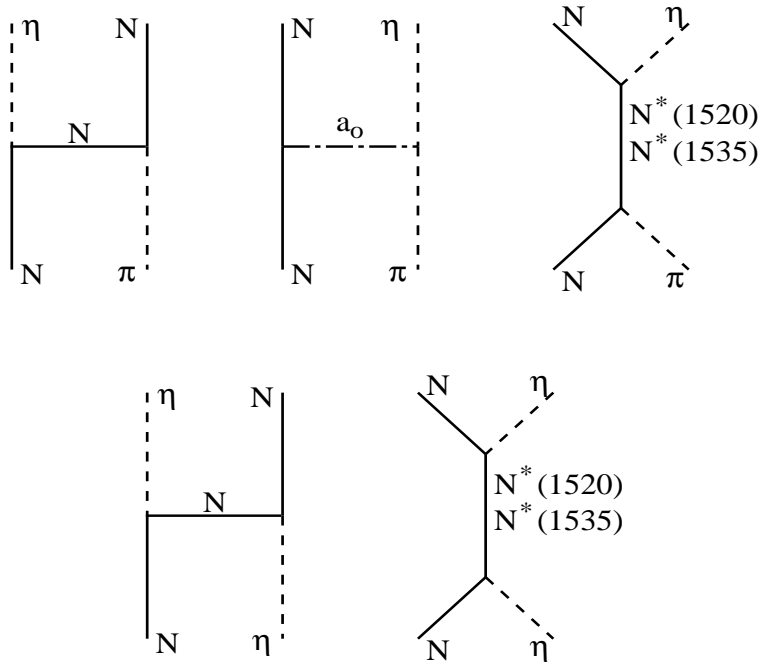


FIG. 1

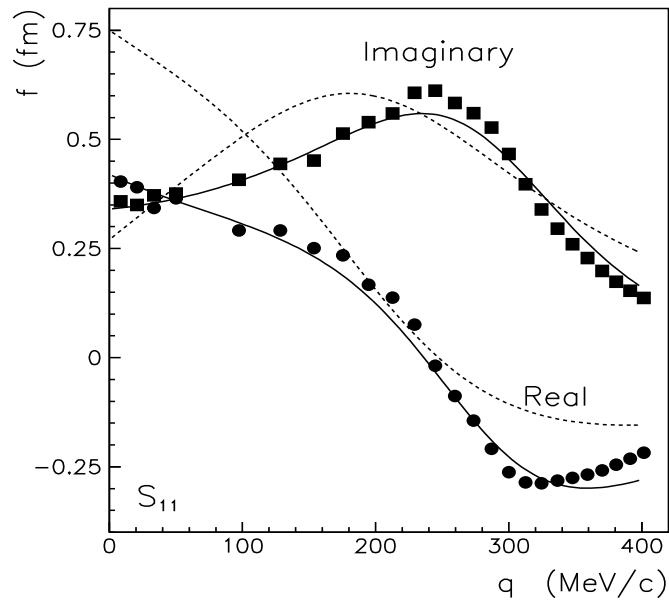


FIG. 2

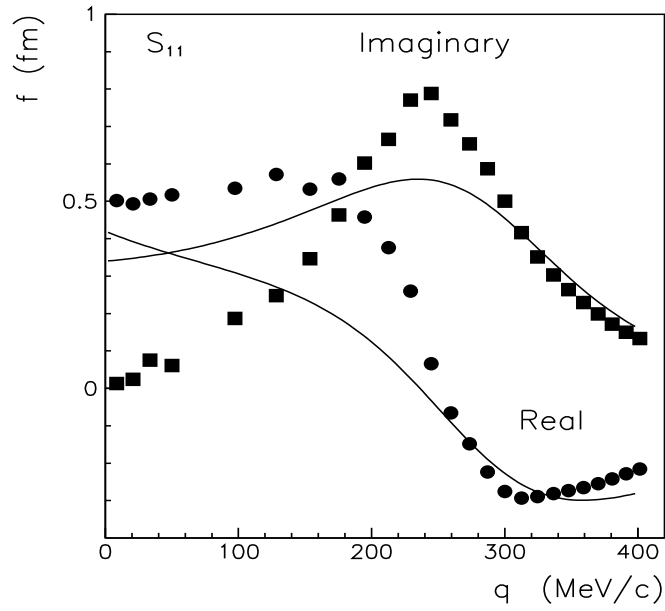


FIG. 3

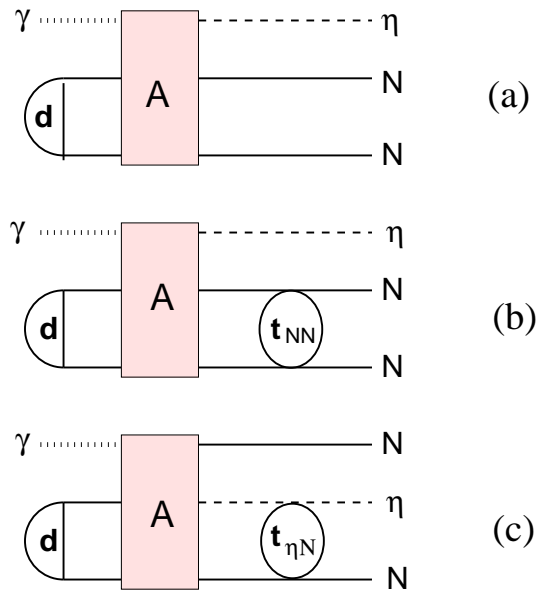


FIG. 4

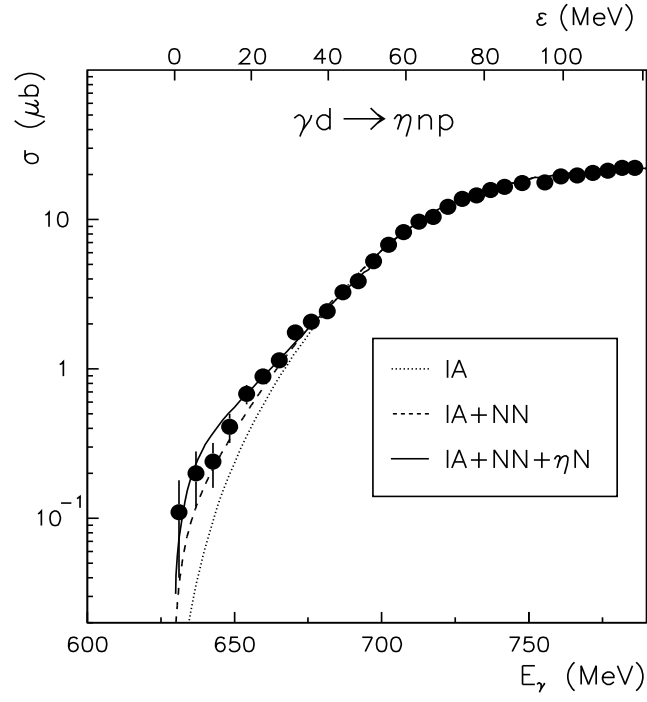


FIG. 5

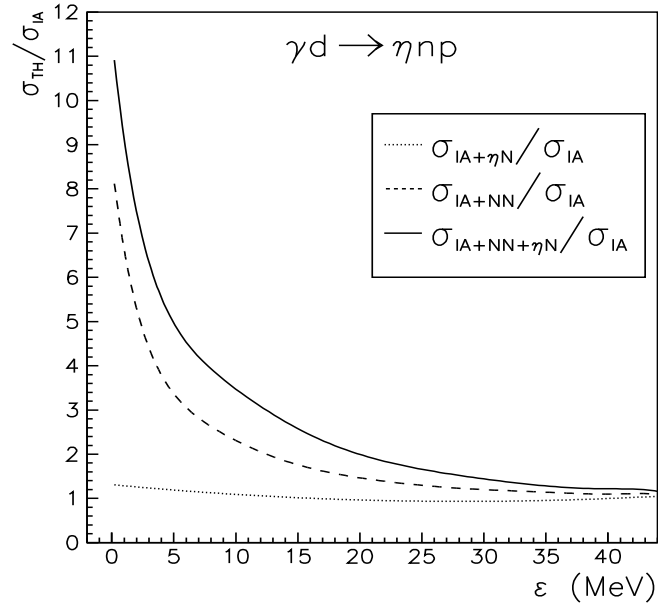


FIG. 6

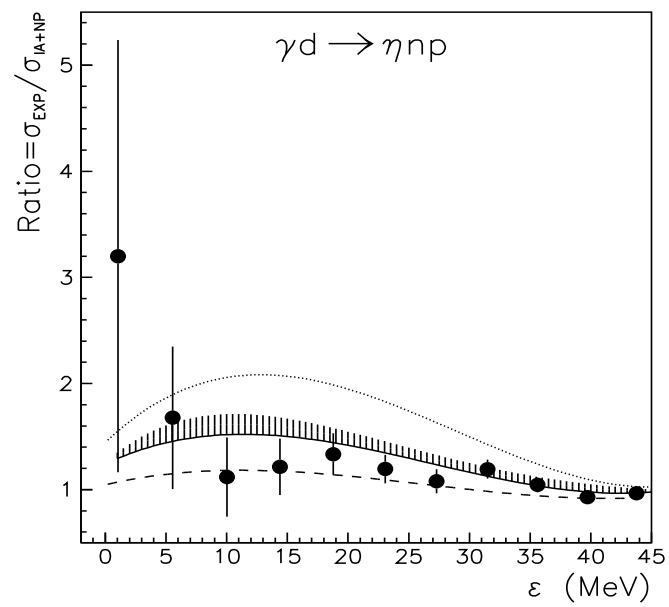


FIG. 7